Experimental and numerical study on square RACFST members under lateral impact loading

You-Fu Yang[*,1], Zhi-Cheng Zhang[1], Feng Fu[2]

1) State Key Laboratory of Coastal and Offshore Engineering, Dalian University of Technology, Dalian, China

2) School of Mathematics, Computer Science & Engineering , Department of Civil Engineering, City University London, Northampton Square, London, UK

Abstract:

In this paper, experimental and numerical studies were carried out to investigate the performance of recycled aggregate concrete (RAC) filled square steel tubular members under lateral impact loading. A total of eleven specimens, including eight RAC filled steel tubular (RACFST) specimens and three normal concrete filled steel tubular (CFST) counterparts, were tested using drop-weight impact test rigs with fixed boundary conditions at both ends. The parameters studied were: recycled coarse aggregate (RA) replacement ratio, axial compressive load ratio and height of the drop-weight. The failure mode and local damages of the specimens were extensively investigated. The experimental results show that square RACFST specimens have the almost equivalent lateral impact resistance as normal CFST counterparts. Failure mode of steel tube is commonly indentation at the impacted area and buckling at the compression side of the section near the mid-span and the supports. Cracking under tension as well as crushed under compression of core concrete are observed at the mid-span and the location near the supports. A finite element analysis (FEA) model was also developed for simulating the performance of square RACFST members under lateral impact loading, and the predicted responses using the FEA model were in good agreement with the experimental results.

Keywords: Recycled aggregate concrete filled steel tube (RACFST); Square section; Lateral

*Corresponding author. Tel.: 86-411-8470 8510; Fax: 86-411-8467 4141.
E–mail address: youfuyang@163.com (Dr. You-Fu Yang).

impact loading; Time history response; Impact load; Finite element analysis (FEA)

Nomenclature

B	external width of square steel tube
CFST	concrete filled steel tube
h	height of the drop-weight
L	total length of the specimen
L_0	clear length between two supports
n	axial compressive load ratio
N_0	axial compressive load
NC	normal concrete
NA	natural coarse aggregate
P	impact load
$P_{k,e}$	experimental peak of impact load
$P_{s,p}$	predicted plateau of impact load
$P_{s,e}$	experimental plateau of impact load
r	recycled coarse aggregate replacement ratio
RA	recycled coarse aggregate
RAC	recycled aggregate concrete
RACFST	recycled aggregate concrete filled steel tube
t	time
$t_{d,e}$	experimental duration from starting impacting to reaching the maximum displacement
$t_{d,p}$	predicted duration from starting impacting to reaching the maximum displacement
t_s	wall thickness of steel tube
W	initial kinetic energy of the drop-weight
u	displacement
u_m	displacement at the mid-span
$u_{mm,e}$	experimental maximum dynamic displacement at the mid-span
$u_{mm,p}$	predicted maximum dynamic displacement at the mid-span

u_{mr} residual displacement at the mid-span

1. Introduction

In modern construction project, concrete filled steel tube (CFST) exhibits various advantages: steel tube can effectively constrain its core concrete, thus delay the longitudinal cracking of concrete under compression and improve the plastic deformation capability of core concrete; and at the same time core concrete can delay or prevent premature local buckling of steel tube. As a result, CFST has higher bearing capacity, better ductility and toughness, shorter construction time and better fire resistance compared with single steel tube or core concrete, and it has been widely used in construction practice (Zhao et al. 2010)[1]. However, CFST members may be subjected to accidental or intentional transverse impact loads such as the strike of vehicles and the impact of explosive events, which will seriously damage CFST members and even lead to the collapse of an entire structure.

The behaviour of composite members with steel tube and fillings subjected to lateral impact loads has been experimentally and theoretically investigated by several researchers. Shan et al. (2007)[2] investigated the behaviour of CFST stub columns with the impact loads applied axially by a high-speed gas gun, and the impact responses from tests were used to evaluate the rationality of the analytical results using LS-DYNA. Bambacha et al. (2008)[3] presented an experimental and analytical study on steel hollow sections and CFST beams subjected to transverse impact loads, and a design procedure was proposed. Huo et al. (2009)[4] investigated the impact resistance of small-size micro-concrete-filled steel tubes at elevated temperatures up to 400 ^{o}C using a spilt Hopkinson pressure bar, and a simplified calculation method for the impact resistant capacity of CFST at elevated temperatures was proposed. Bambach (2011)[5] investigated the general behaviour of concrete filled carbon and stainless steel tubular columns under transverse impact loads using the finite element models validated by the tests, and then suggested a design procedure for such members. Based on the combination of experimental results, numerical simulation using LS-DYNA and theoretical analysis, Qu et al. (2011)[6] developed a simplified analytical model for

circular CFST columns with fixed-simple supported ends subjected to lateral impact loading, and the proposed model could well predict the maximum deflection of CFST specimen under lateral impacts. Remennikov et al. (2011)[7] presented the results of experimental and numerical studies on the behaviour of mild and stainless steel square hollow section filled with rigid polyurethane foam and concrete subjected to transverse impact loads. Deng et al. (2012)[8] investigated the failure modes and local damages of the simply supported CFST, steel post-tensioned CFST and steel fiber-reinforced concrete filled tube under lateral impacts, and the tests were carried out by an instrumented drop-weight impact facility. Furthermore, to evaluate the dynamic plastic moment capacity of circular CFST beams under lateral impacts, Deng and Tuan (2013)[9] developed an algorithm based on theoretical sectional analysis (TSA), and a procedure using TSA was finally proposed to assist engineers in designing simply supported circular CFST beams under lateral impacts. Yousuf et al. (2013)[10] presented the comparative results of the experimental and finite element modelling of hollow and concrete-filled stainless steel tubular columns under lateral static or impact loading. Wang et al. (2013)[11] reported the studies on the performance of circular CFST members under transverse impact loads, and both experimental and finite element analysis results were presented and analysed. Han et al. (2014)[12] experimentally and theoretically investigated the impact resistant behaviour of high strength concrete filled steel tubular members, and further developed a simplified model for predicting the flexural strength of CFST members under lateral impact loading.

In recent years, recycled aggregate concrete (RAC) technology has become one of the effective measures to develop green concrete, achieve sustainable development of building, resources and environment and build a resource-saving society, considering that production of recycled aggregates by recycling of the waste concrete can promote the reuse of waste materials and further protect the natural aggregate resources. RAC filled steel tube (RACFST) can be considered as a new type of composite construction technique (Yang and Han 2006)[13]. There have been a number of studies on the static and cyclic behaviour of RACFST members (Yang and Han 2006; Yang et al. 2009;

Yang and Zhu 2009; Yang and Ma 2013)[13-16], and the results show that RACFST members generally have the similar properties as CFST members. The investigation on the behaviour of this type of member under impact loading is a very important issue for ensuring the safety of RACFST structures. However, little research on the behaviour of RACFST members subjected to accidental loads such as collisions, impacts, terrorist bombings, etc. has been done so far.

Based on the aforementioned information, it is clear that the study on the performance of RACFST members under lateral impact loading is limited. This paper presents an experimental and theoretical investigation on the behaviour of square RACFST members subjected to lateral impact loading. In this study, the influence of recycled coarse aggregate (RA) replacement ratio, axial compressive load ratio and height of the drop-weight on the impact resistance behaviour of square RACFST members was experimentally investigated. Moreover, a finite element analysis (FEA) model was developed to predict the response of square RACFST members under lateral impact loading, and the accuracy of the model was evaluated by comparison with the experimental results.

2. Experimental Program

2.1. Material Properties

The steel tube used in the tests was cut from a pre-fabricated cold-formed square hollow section with the average wall thickness (t_s) of 2.45 mm. The properties of steel were tested by using three tensile coupons randomly taken from the flat part of square hollow section. From the tests, the average yield strength, tensile strength, modulus of elasticity and Poisson's ratio of steel were found to be 370.8 MPa, 446.5 MPa, 1.98×10^5 N/mm^2 and 0.267, respectively. The average strain at rupture (elongation), which reflects the ductility of steel, is 18.7% with a standard deviation of 1.8%.

RA was obtained by crushing the waste concrete in the laboratory using a small jaw crusher, and the cube compressive strength of the waste concrete was about 60 MPa. The maximum size of RA and natural coarse aggregate (NA) was 20 mm and 25 mm. The methods for determining the water absorption rate and crushing value in GB/T 14685-2011 [17] were adopted. The water

absorption rate of RA and NA was 8.49% and 0.78%, respectively and the crushing value of RA and NA was 29.4% and 11.5%, respectively. Three types of concrete, including one type of normal concrete (NC) with natural aggregates as a counterpart, two types of RAC with RA replacement ratio (r) of 50% and 100%, were produced in the tests, where r was defined as the ratio of RA mass to the mass of all coarse aggregate. The mix design of all concrete was kept as the same, and the NC counterpart was designed with a mean cube compressive strength of approximately 40 MPa at 28-day. Furthermore, to ensure the workability of RAC, the RA was pre-wet to attain the saturated surface dry (SSD) condition before mixing concrete, considering that the water absorption of RA is higher than that of NA. To monitor the cube compressive strength (f_{cu}) and elastic modulus (E_c) of concrete, 150 mm cubes and 150 mm × 300 mm prisms were cast and cured in conditions similar to the tested specimens. The mix design and properties of fresh concrete are presented in Table 1, where $f_{cu,28}$ and $f_{cu,test}$ are the mean cube compressive strength at 28-day and when the loading tests conducted, respectively. It can be seen that the slump of RAC with r of 100% is more than twice that of NC and RAC with r of 50%, which have the slump of 35 mm. This result may be caused by the additional water in RAC with r of 100% because of the difficulty in accurately controlling the SSD condition. It can also be seen from Table 1 that f_{cu} and E_c of RAC are lower than those of the corresponding NC, and higher r results in lower f_{cu} and E_c. Similar results were reported by Yang and Han (2006)[13].

2.2. Specimens

Eleven square specimens, including eight RACFST members and three CFST counterparts, were tested under lateral impact loading produced by an instrumented drop-weight impact tester and the tube of each specimen was welded to two square 12 mm thick steel base plates. The information of the specimens investigated in the tests is listed in Table 2, where B is the external width of square steel tube, L is the total length of the specimen, L_0 is the clear length between two supports, h is the height of the drop-weight, N_0 is the applied axial compressive load, n

($=N_0/N_u$, where N_u is the stability bearing capacity of RACFST members (Yang and Hou 2014)[18]) is the axial compressive load ratio, W is the initial kinetic energy of the drop-weight, $t_{d,e}$ is the experimental duration from starting impacting to reaching the maximum displacement, $P_{k,e}$ is the experimental peak of impact load, $P_{s,e}$ is the experimental plateau of impact load, $u_{mm,e}$ is the maximum dynamic displacement at the mid-span during the tests, and u_{mr} is the residual displacement at the mid-span after impacting. The main parameters considered in the tests include:

- RA replacement ratio, r: from 0 (CFST) to 100%,
- Axial compressive load ratio, n: from 0 to 0.33, and
- Height of the drop-weight, h: from 2 m to 6 m.

In Table 2, 'NC', 'RAC1' and 'RAC2' in the first part of specimen label denotes the filling concrete of NC, RAC with r of 50% and RAC with r of 100% respectively, the middle part of specimen label indicates the axial compressive load ratio, and the numbers in the last part of specimen label refer to the height of the drop-weight.

2.3. Impact Tests

The tests were carried out on an instrumented drop-weight impact tester. The effective height of the tester is 12.6 m and the corresponding maximum impact velocity is 15.7 m/s. Details of the tester were presented in Wang et al. (2013)[11]. The fluted H-shaped weight was made of ASTM 1045 quality carbon structural steel. The impact head was made of chrome 15 with the hardness of 64HRC, and the dimension of the effective contact surface is 30 mm×80 mm. The dynamic load cell was installed between the impact head and the weight to record the time history of impact loads. The drop-weight consists of the weight, the dynamic load cell and the impact head, which are connected to each other using high-strength bolts, and the mass of the drop-weight is 238.16 kg in the tests. The above instrumentation allows free fell of the drop-weight from different height to produce lateral impact on the tested specimens.

The specimen was fixed supported at both ends, and the supports consisted of the upper and

lower half rings and the base plate fixed to a steel working platform. A schematic view of the test assembly is shown in Fig. 1. Meanwhile, to simulate the combined compression and bending of a structural member under lateral impact loading in reality, 100 kN or 200 kN axial compressive load was applied to the ends of six RACFST specimens and two CFST counterparts, as shown in Table 2. The device for applying axial compressive force was composed of close channel frame, load axle, load ring, linear bearings, disc springs, hydraulic jack, load transducer and other necessary components, and the linear bearings in the right support were used to restrict the displacement in lateral direction and permit deforming only in axial direction. The compressive load could be ensured less loss as far as possible during the lateral impacting by adoption of disc springs (Wang et al. 2013; Han et al. 2004)[11,12]. The monitored results showed that, the axial compressive load fluctuated and attenuated during the impact load tests and it is noticed that the maximum variation range was 20% of the applied constant axial compressive load.

During the tests, the specimen was placed in the test assembly with the left end restricted in the longitudinal direction, and then the compressive load was applied to the right end of the axially loaded specimens. The drop-weight was released at different height to hit the specimen at the mid-span and the time history of impact load was recorded by the dynamic load cell installed in the drop-weight. Simultaneously, six displacement markers were set on the side surface of the specimens to trace the development of the lateral displacements and to obtain the final lateral displacement (residual displacement), as shown in Fig. 2. Moreover, an i-SPEED 3 high-speed video camera produced by OLYMPUS Company was used to record the specimen destruction process, and the digital video acquisition recorded the tests at a speed of 3000 frames per second.

3. Test Results and Discussion

The response of RACFST specimens and the CFST counterparts under lateral impact loading was initially dominated by a combination of local deformation and global bending, and subsequently, the lateral displacements increased quickly. During the impact loading tests, the responses of the tested specimens with both ends fixed showed the conventional plastic failure

mechanism due to bending, and three plastic hinges were formed along the span of the specimen, including one at each end and one at the mid-span. The remaining part of the specimen was still flat. The typical mechanism behaviour is shown in Figs. 3 and 4. Fig. 3 shows the displacement (u) developments of specimen RAC2-0.165-6 with 1 ms interval till reaching the maximum dynamic displacement ($u_{\mathrm{mm,e}}$), where x is the distance away from the left support and the curves were traced over pictures taken from the video camera (Fig. 4). The failure proceeded from the initial contact between impact head and specimen to the time impact load basically reaching a stable stage. It can be found from the movement of displacement markers (white points in Fig. 4) that, the displacement of specimen becomes more and more evident with time (t) increasing.

Fig. 5 shows the failure pattern of the specimens after the completion of impact tests. It can be seen that, in general, the indentation of steel tube appears at the impact position and the shape of the square cross section is no longer maintained. A final "V" shape of the specimens is produced within the clear span except for specimen RAC1-0.16-2. The steel tube buckles on both sides of the impact location and at the compression zone near the supports (position of the arrows), and the value and range of buckling deformation are obviously determined by the height of the drop-weight. Moreover, cracks at the tension zone near the impact location (position of the dashed oval) were observed on the steel tube of RACFST specimens without axial compressive load. This phenomenon may be due to the fact that core RAC in RACFST can not provide adequate restrain to the steel tube under lateral impact loading as the strength and elastic modulus of RAC are lower than those of NC.

In general, the failure mode of RACFST specimens under lateral impact loading can be divided into three categories with variation of r, n and h, as summarised in Table 1 and shown schematically in Fig. 6. It can be seen that, for axially loaded specimen with a small height of the drop-weight (i.e. h=2 m), only local buckling of steel tube were observed at the compression side of the section near the mid-span [Fig. 6(a)]. For axially loaded specimen with an increasing height of the drop-weight (i.e. h=4 m or 6 m), local buckling of steel tube also appears at the compression

side of the section near the supports [Fig. 6(b)] due to the increase of impact energy. However, for specimens without axial compressive load applied, tensile facture of steel tube at the tension side of the mid-span section is further developed [Fig. 6(c)], which is also different from the failure mode of the CFST counterparts. These can be explained that, while being subjected to lateral impact loading, the existence of axial compressive load can restrain the development of tensile strain in the tube and improve the plastic deformation capability of core RAC in RACFST specimens.

After the impact tests, half of the steel tube of the specimens was cut open to inspect the failure pattern of core concrete inside, as shown in Fig. 7(a). It is shown that tensile cracks occur at the tension side of the sections near the supports [Fig. 7 (b) and (d)] and at the mid-span [Fig. 7 (c)]. At the same time, concrete core is commonly crushed at the mid-span and the location near the supports. The concrete core between mid-span and the supports is remained fairly intact, and there is no evident shear crack observed in the core concrete due to the effective confinement provided by steel tube. It can also be found from Figs. 5 and 7 that, shear failure including punching shear failure of steel tube and core concrete at the mid-span occurs as the dimensions of the effective contact surface of the drop-weight are smaller than those of the upper surface of the specimens and as the elastic modulus of core concrete is lower than that of the outer steel tube. Moreover, the shear failure including punching shear failure becomes more evident for specimens with larger axial compressive load ratio and height of the drop weight. This can be attributed to the difference in the stress state because of the axial compressive load applying and the increase of impact energy.

The most important data recorded during the impact tests are the time history of impact load (P) applied on the specimen, and the typical time history of impact loads of a specimen is shown in Fig. 8. It can be seen that, the impact load (P) versus time (t) history curve can be generally divided into three phases, namely oscillation stage (point O to A), stabilization stage (point A to B) and attenuation stage (point B to C). The determination of stabilization stage (points A and B) is based on that the variation range of P is less than 5 kN within 1 ms after point A and at point B the sudden change happens to slope of $P-t$ curve. The impact load reaches the maximum value

in a short time and then fast decays in the oscillation stage, and the impact load is generally constant in the stabilization stage. Finally, the impact load is gradually reduced to zero in the attenuation stage when the impact energy is mostly dissipated. For all specimens, the experimental peak of impact load ($P_{k,e}$) is determined as the maximum force recorded in the tests. The average force within the first 5 ms of stabilization stage of $P-t$ history curve is treated as the plateau of impact load ($P_{s,e}$) considering that the fluctuation of P is small within this period and the impact load starts to attenuate after this period due to the influence of potential interference factors. Both $P_{k,e}$ and $P_{s,e}$ are presented in Table 2.

The impact load (P) versus time (t) history curve of the specimens is illustrated in Fig. 9. It is shown that, in general, the difference in the oscillation stage of $P-t$ history curves is not evident. However, significant difference was observed in the stabilization stage and attenuation stage, and the forces in the stabilization stage and the duration from point A to C (see Fig. 8) change with the variation of r, h and N_0.

The time histories of mid-span displacement (u_m) of RACFST specimens and the CFST counterparts are shown in Fig. 10. The experimental maximum dynamic displacement ($u_{mm,e}$) at the mid-span is listed in Table 2. It can be seen that, under the same 6-m height of drop-weight (h), RACFST specimens and their CFST counterparts almost have the same responses when the time is less than 0.008 s, and then the u_m-t curves change with the changing of r and n. However, the more difference was observed in u_m-t curves for specimens without axial compressive load than that in axially loaded specimens. For the specimens without axial compressive load, the u_m-t curve of RACFST specimens is higher than that of the corresponding CFST specimen due to the fracture of their steel tube at the tension side of the mid-span section (see Fig. 5(a)); however, for axially loaded specimens with the same h, the u_m-t curve of RACFST specimens is generally lower than that of the CFST counterparts, i.e. RACFST specimens have a better deformation-resistant capability. This result may be explained by the fact that, the surface of RA is

coarser than that of NA (Hansen 1992)[19], and meanwhile the bond action between RA and hydration products of RAC is further improved because of the existence of axial compressive load. It can also be found that, the axially loaded RACFST specimens have a higher $u_m - t$ curve than RACFST specimens without axial compressive load; however, for CFST specimens the axial compressive load dramatically increases its mid-span displacement. This phenomenon may be due to the fact that the influence of the second-order effect on CFST specimens is more significant than that on RACFST specimens since core concrete in RACFST specimens has a coarser surface between RA and hydration products than that in CFST specimens. Moreover, Fig. 10(d) shows that, for RACFST specimens under the same axial compressive load ratio (n), the $u_m - t$ responses increase obviously with increase of h owing to the increase of impact energy.

The effect of RA replacement ratio (r), axial compressive load ratio (n) and height of the drop-weight (h) on the measured peak and plateau of impact load ($P_{k,e}$ and $P_{s,e}$) is demonstrated in Fig. 11. It can be seen that, except for $P_{k,e}$ of CFST specimens, $P_{k,e}$ of RACFST specimens and $P_{s,e}$ of all specimens decrease with increase of n because of the existence of second-order effect of axial compressive load. Due to the lower compressive strength and elastic modulus of RAC compared with NC, $P_{k,e}$ and $P_{s,e}$ of RACFST specimens are 5.4-28.9% and 1.0-11.2% lower than those of the corresponding CFST specimens, respectively. In general, $P_{k,e}$ increases with increase of h due to the increase of impact energy; however, similar to CFST specimens in Wang et al. (2013)[11] and Han et al. (2014)[12], h has little effect on $P_{s,e}$ of RACFST specimens owing to the fact that the time history responses of P at the stabilization stage is little related to h.

Figs. 12 and 13 show the effect of typical parameters on the residual displacement at the mid-span (u_{mr}) and the experimental duration from starting impacting to reaching the maximum displacement ($t_{d,e}$). It can be seen that, h has a significant influence on u_{mr} and $t_{d,e}$ of the specimens due chiefly to its determination on the impact energy; however, r and n do not have

consistent effect on u_{mr} and $t_{d,e}$ of RACFST specimens and the CFST counterparts under the same h value. As mentioned above, the existence of axial compressive load will affect the transition zone and bond action between RA and hydration products of RAC in RACFST specimens and this will determine the performance of RACFST specimens under lateral impact loading.

4. Finite element analysis (FEA) model

4.1. General description of the FEA model

To simulate the responses of square RACFST members subjected to lateral impact loading at the mid-span, a nonlinear finite element analysis (FEA) model was developed using ABAQUS software [20]. In the simulation, applying axial compressive loads was modelled by Abaqus/Standard solver, and then the explicit solver was used to model the performance under lateral impact loading.

In this study, the relevant static and strain rate properties of steel were same as those presented in Wang et al. (2013)[11]. The damaged plasticity model in ABAQUS was adopted to simulate the complicate nonlinear behaviour of core concrete. The static stress–strain relationship of RAC under compression was derived from the model of NC presented in Han et al. (2007) [21] by considering the effect of r on the peak stress and the peak strain (Zhang 2014)[22]:

$$\sigma_{0,r} = \sigma_{0,n} \cdot (1 - 0.28r + 0.08r^2) \tag{1}$$

$$\varepsilon_{0,r} = \varepsilon_{0,n} \cdot [1 + r/(65.715r^2 - 109.43r + 48.989)] \tag{2}$$

where, $\sigma_{0,r}$ ($\varepsilon_{0,r}$) and $\sigma_{0,n}$ ($\varepsilon_{0,n}$) are the peak stress (strain) of RAC and the corresponding NC, respectively. The static stress–strain relationship of NC under tension given in Shen et al. (1993)[23] was adopted as the model for core RAC, i.e. the effect of r was not considered. Till now, there is no model for considering the effect of strain rate on RAC. Thus, the method with the effect of strain rate on NC considered in CEB-FIP (1993)[24], which had been successfully used in the modelling of CFST members under lateral impacting loading (Han et al. 2013, 2014)[11][12], was temporally adopted in this study.

In the model, the steel tube and core concrete were simulated by 4-node reduced-integration three-dimensional shell elements (S4R) and 8-node reduced-integration three-dimensional brick elements (C3D8R), respectively. The detailed information of the interface between the steel tube and core concrete could be found in Han et al. (2007) [21]. The disc springs in the tests were simulated by a spring element with two point connection, and the stiffness used for the spring element was 6×10^6 N/mm. The drop-weight was modelled by 4-node three-dimensional rigid elements (R3D4). Moreover, the drop-weight was simplified to be a rigid surface with the same dimensions as the impacted surface since the shape of the drop weight almost unchanged during the impacting tests. The mesh convergence studies showed that, local mesh encryption was necessary in the range of contacting between the drop-weight and the member to ensure the computational efficiency and to improve the accuracy of prediction. The boundary conditions at one end were 'fixed' with all degree of freedoms restricted, and at the other end all degree of freedoms was restricted except for the longitudinal direction. Furthermore, the geometric nonlinearity (large deformation) is assumed in the proposed model to include the second-order effect. The adopted meshing and boundary conditions for a typical RACFST member is demonstrated in Fig. 14. The Initial velocity (v_0) considered in the tests was defined for the drop-weight, and the responses of RACFST members under lateral impact loading after each step could be obtained from the equilibrium equations.

4.2. Verifications of the FEA model

Fig. 15 shows the predicted failure patterns of the tested specimens. It can be seen from Fig. 15 and Fig. 5 that, in general, the FEA model can well predict the deformation of RACFST specimens and the local buckling of steel tube. The comparison between the predicted and tested $P-t$ and $u_{\mathrm{m}}-t$ curves is illustrated in Fig. 16 and Fig. 17, respectively. It can be found that a reasonably good agreement is obtained between both results. However, the predicted $P-t$ history curve of specimens RAC1-0-6 and RAC2-0-6 has a short duration time as the tensile fracture of steel is not considered in the FEA model. In general, the predicted u_{m} are slightly larger than the test results

after reaching the maximum dynamic displacement. This can be attributed to the fact that the FEA model can not simulate the effect of air resistance, frition between devices and environmental interference. The comparisons of P_s, t_d and u_{mm} between the predicted and experimental results are demonstrated in Fig. 18, where $P_{s,p}$, $t_{d,p}$ and $u_{mm,p}$ are the predicted plateau of impact load, duration from starting impacting to reaching the maximum displacement and maximum dynamic displacement at the mid-span, respectively, and MV and SD represent mean value and standard deviation, respectively. As could be found, the mean values of $P_{s,p}/P_{s,e}$, $t_{d,p}/t_{d,e}$ and $u_{mm,p}/u_{mm,e}$ are respectively 0.853, 1.049 and 1.085 and the corresponding standard deviations are respectively 0.130, 0.098 and 0.054. In general, a good agreement between the predicted and experimental results was attained.

5. Conclusions

An experimental and numerical investigation on the performance of square RACFST members under lateral impact loading is presented in this study. Based on the observations and analytical results, the following conclusions can be drawn:

(1) RACFST members have the similar lateral impact resistance as CFST counterparts and three stages are observed in the time history curve of impact loads. However, under the same h, the effect of n on the performance of RACFST specimens is different from that of the CFST counterparts.

(2) Failure mode of steel tubes is commonly concave at the impacted area and buckling at the section near the mid-span and the supports, and core concrete is crushed and cracking at the mid-span section and the section near the supports. Moreover, shear failure including punching shear failure of steel tube and core concrete are also observed.

(3) $P_{k,e}$ and $P_{s,e}$ of RACFST specimens are lower than those of the CFST counterparts. For RACFST specimens, $P_{k,e}$ decreases with increase of n and decrease of h, and $P_{s,e}$ decreases with increasing n while h has a moderate effect on $P_{s,e}$. Moreover, r and n have no

consistent effect on $u_{\mathrm{m,r}}$ and t_{d} of RACFST specimens and the CFST counterparts.

(4) The predicted responses of RACFST members under lateral impact loading by the FEA model developed in this study are in good agreement with the experimental observations.

It is clear that the plastic deformation of RACFST members mainly concentrates on the impact position. As a result, the strengthening of the impact parts (e.g. jacket pipe and inner stiffener) is necessary to improve the impact resistance capacity of RACFST members.

Acknowledgements

The studies in this paper are financially supported by the Science Fund for Creative Research Groups of the National Natural Science Foundation of China (51421064), the Natural Science Foundation of Liaoning Province (2013020125) and the Fundamental Research Funds for the Central Universities (DUT12ZD215). The financial support is gratefully acknowledged. The authors also wish to thank Prof. Jian-Ping Lei for his assistance in the tests.

References

[1] Zhao XL, Han LH, Lu H. Concrete-filled tubular members and connections. Oxford: Taylor and Francis; 2010.

[2] Shan JH, Chen R, Zhang WX, Xiao Y, Yi WJ, Lu FY. Behavior of concrete filled tubes and confined concrete filled tubes under high speed impact. Advances in Structural Engineering 2007; 10(2): 209-18.

[3] Bambacha MR, Jama H, Zhao XL, Grzebieta RH. Hollow and concrete filled steel hollow sections under transverse impact loads. Engineering Structures 2008; 30: 2859-70.

[4] Huo JS, Zheng Q, Chen BS, Xiao Y. Tests on impact behaviour of micro-concrete-filled steel tubes at elevated temperatures up to 400°C. Materials and Structures 2009; 42(10): 1325-34.

[5] Bambach MR. Design of hollow and concrete filled steel and stainless steel tubular columns for transverse impact loads. Thin-Walled Structures 2011; 49: 1251-60.

[6] Qu H, Li G, Chen S, Sun J, Sozen MA. Analysis of circular concrete-filled steel tube specimen under lateral impact. Advances in Structural Engineering 2011; 14(5): 941-51.

[7] Remennikov AM, Kong SY, Uy B. Response of foam- and concrete-filled square steel tubes under low-velocity impact loading. Journal of Performance of Constructed Facilities ASCE 2011; 25(5): 373-81.

[8] Deng Y, Tuan CY, Xiao Y. Flexural behavior of concrete-filled circular steel tubes under high-strain rate impact loading. Journal of Structural Engineering ASCE 2012; 138(3): 449-56.

[9] Deng Y, Tuan CY. Design of concrete-filled circular steel tubes under lateral impact. ACI Structural Journal 2013; 110(4): 691-701.

[10] Yousuf M, Uy B, Tao Z, Remennikov A, Liew JYR. Transverse impact resistance of hollow and concrete filled stainless steel columns. Journal of Constructional Steel Research 2013; 82: 177-89.

[11] Wang R, Han LH, Hou CC. Behavior of concrete filled steel tubular (CFST) members under lateral impact: Experiment and FEA model. Journal of Constructional Steel Research 2013; 80: 188-201.

[12] Han LH, Hou CC, Zhao XL, Rasmussen KJR. Behaviour of high-strength concrete filled steel tubes under transverse impact loading. Journal of Constructional Steel Research 2014; 92: 25-39.

[13] Yang YF, Han LH. Compressive and flexural behaviour of recycled aggregate concrete filled steel tubes (RACFST) under short-term loadings. Steel and Composite Structures 2006; 6(3): 257-84.

[14] Yang YF, Han LH, Zhu LT. Experimental performance of recycled aggregate concrete-filled circular steel tubular columns subjected to cyclic flexural loadings. Advances in Structural Engineering 2009; 12(2): 183-94.

[15] Yang YF, Zhu LT. Recycled aggregate concrete filled steel SHS beam-columns subjected to cyclic loading. Steel and Composite Structures 2009; 9(1): 19-38.

[16] Yang YF, Ma GL. Experimental behaviour of recycled aggregate concrete filled stainless steel tube stub columns and beams. Thin-Walled Structures 2013; 66: 62-75.

[17] GB/T 14685-2011. *Pebble and crushed stone for construction*. Beijing: Standards Press of China; 2011. (in Chinese)

[18] Yang YF, Hou C. Behaviour and design calculations of recycled aggregate concrete filled steel tube (RACFST) members. Magazine of Concrete Research, Forthcoming 2014.

[19] Hansen TC. Recycled aggregates and recycled aggregate concrete second state-of-the-art report developments 1945-1985. Materials and Structures 1986; 19(3): 201-246.

[20] ABAQUS. *ABAQUS Standard User's Manual*, Version 6.7. Dassault Systèmes Corp., Providence, RI, USA, 2007.

[21] Han LH, Yao GH, Tao Z. Performance of concrete-filled thin-walled steel tubes under pure torsion. Thin-Walled Structures 2007; 45(1): 24-36.

[22] Zhang ZC. Impact resistant behavior of recycled aggregate concrete-filled steel tubular members [dissertation]. Dalian: Dalian University of Technology; 2014.

[23] Shen JM, Wang CZ, Jiang JJ. Finite element analysis of reinforced concrete structures and limit state analysis of reinforced concrete plates and shells. Beijing: Tsinghua University Press; 1993.

[24] Comite Euro-International du Beton. CEB-FIP Model Code 1990. Trowbridge, Wiltshire, UK: Redwood Books; 1993.

Figures:

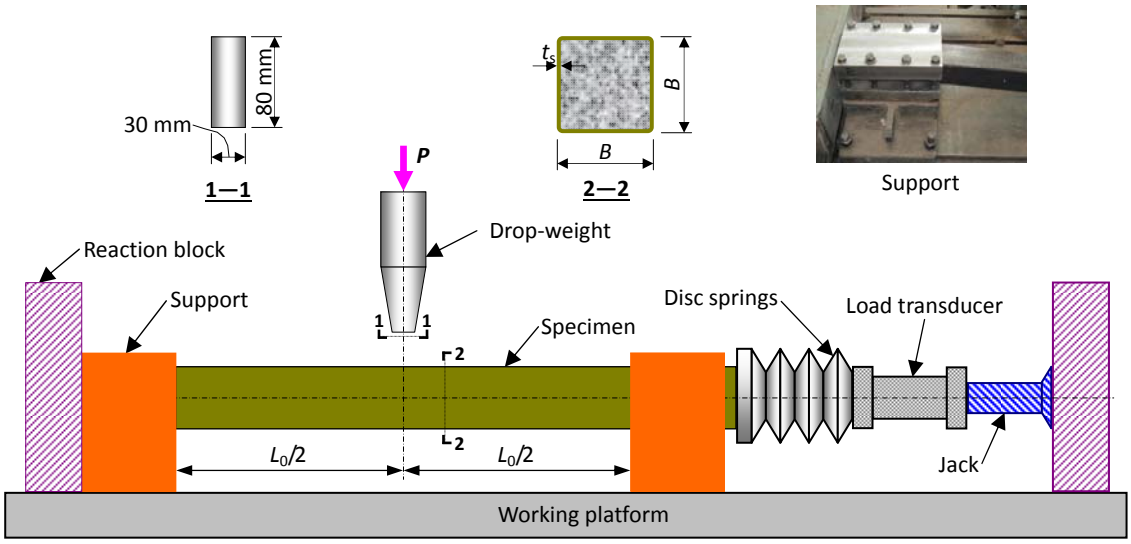

Fig. 1. A schematic view of the test assembly.

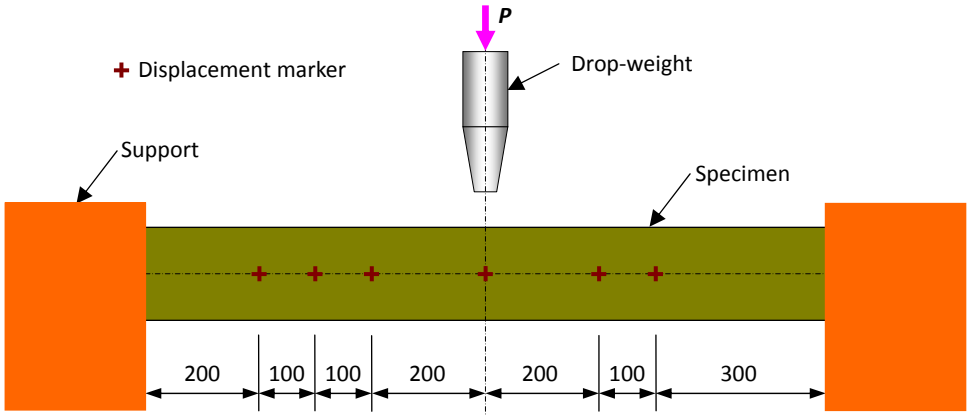

Fig. 2. Distribution of displacement markers and strain gauges. (unit: mm)

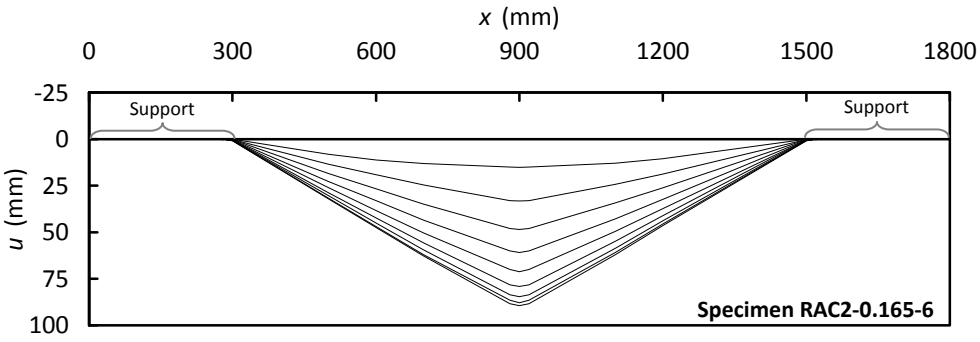

Fig. 3. Typical displacement developments with 2 ms interval.

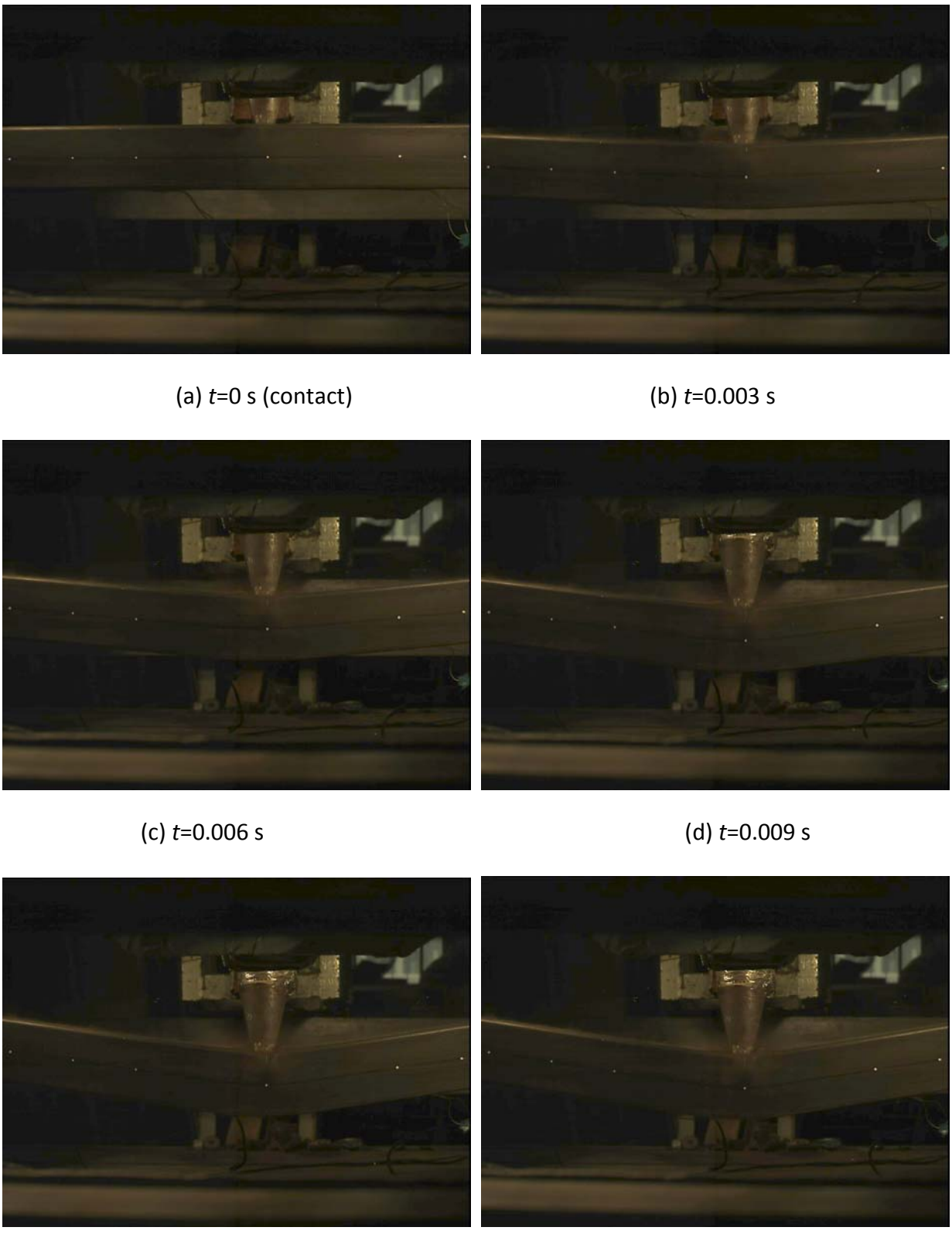

(a) *t*=0 s (contact) (b) *t*=0.003 s

(c) *t*=0.006 s (d) *t*=0.009 s

(e) *t*=0.012 s (f) *t*=0.016 s

Fig. 4. Failure process of specimen RAC2-0.165-6.

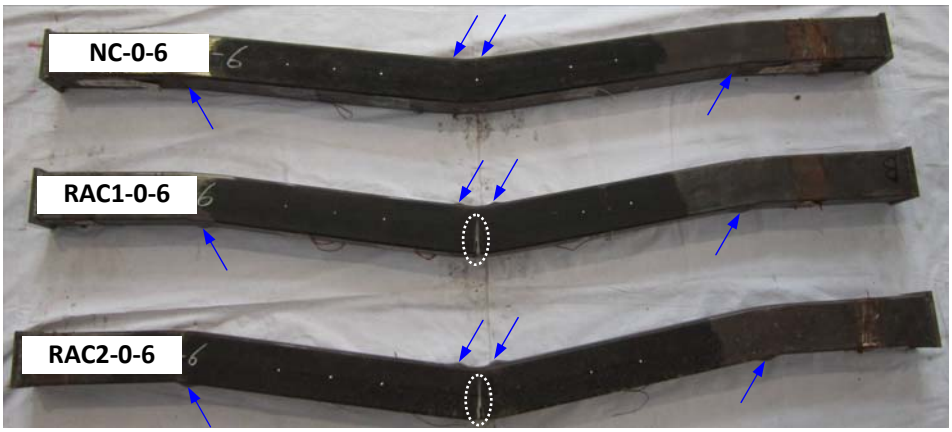

(a)

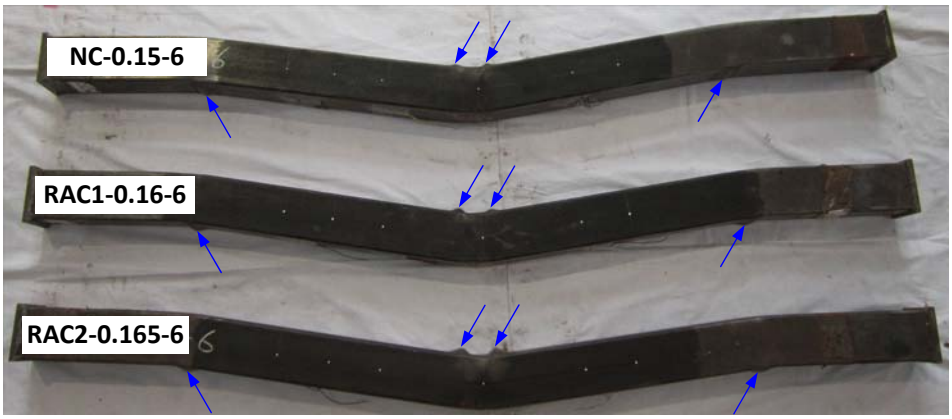

(b)

Fig. 5. Continued

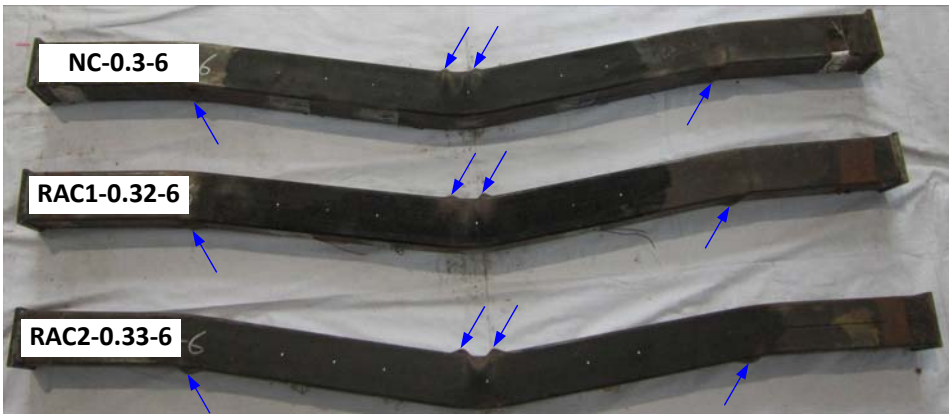

(c)

(d)

Fig. 5. Failure pattern of the specimens.

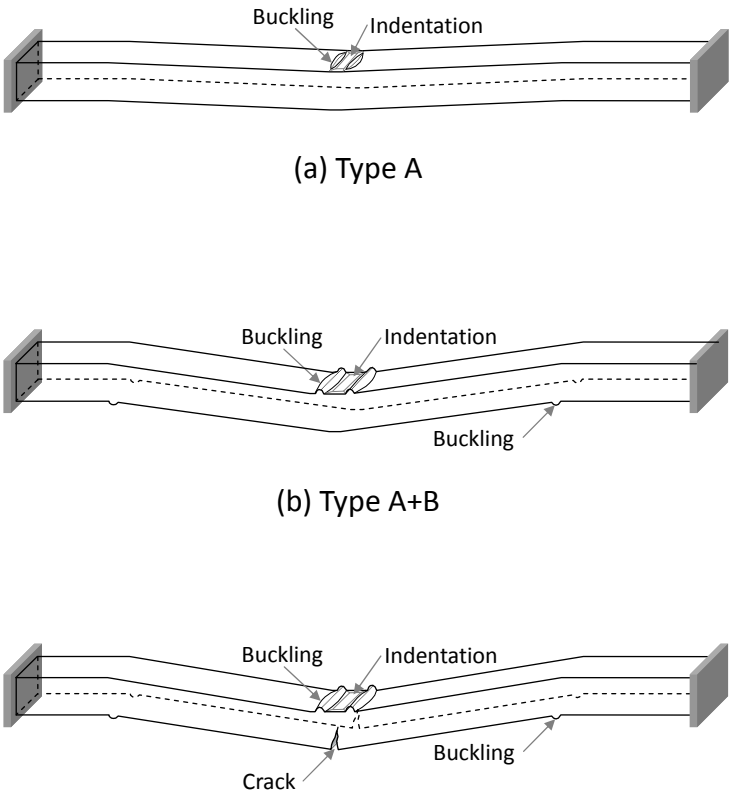

Fig. 6. Failure mode of RACFST specimens under lateral impact loading.

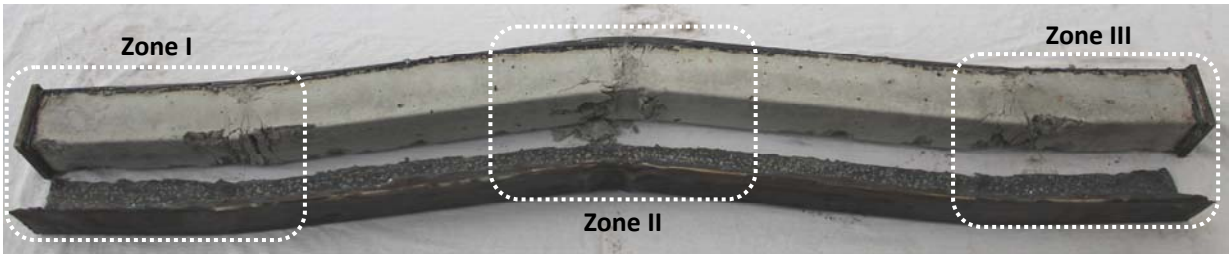

(a) Overall pattern

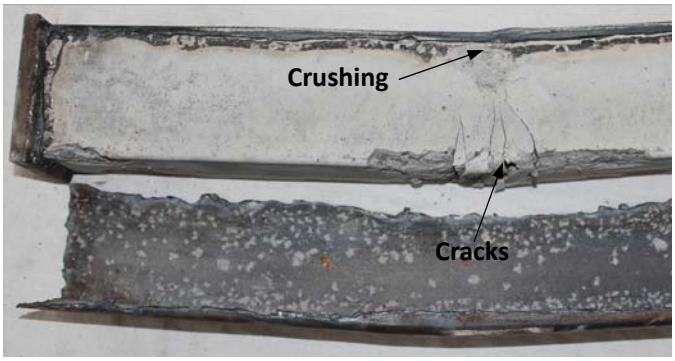

(b) Zone I

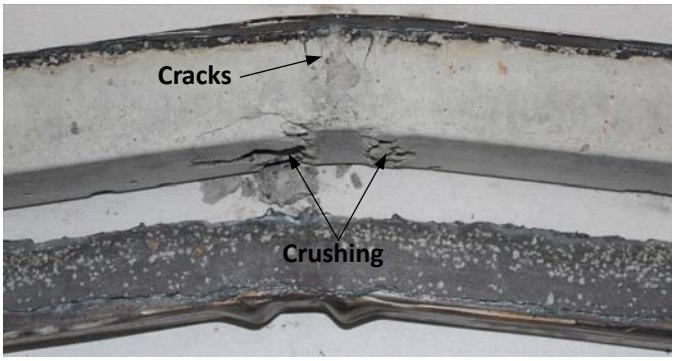

(c) Zone II

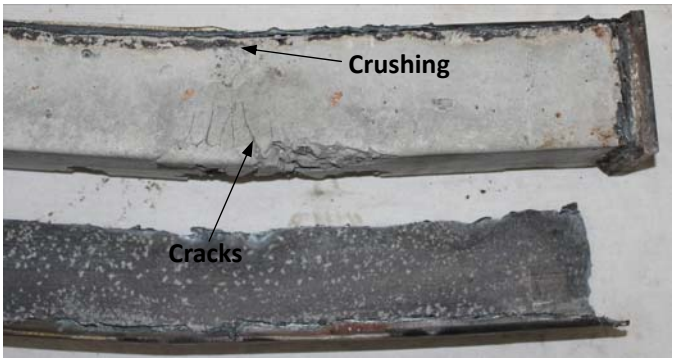

(d) Zone III

Fig. 7. Typical failure pattern of core concrete.

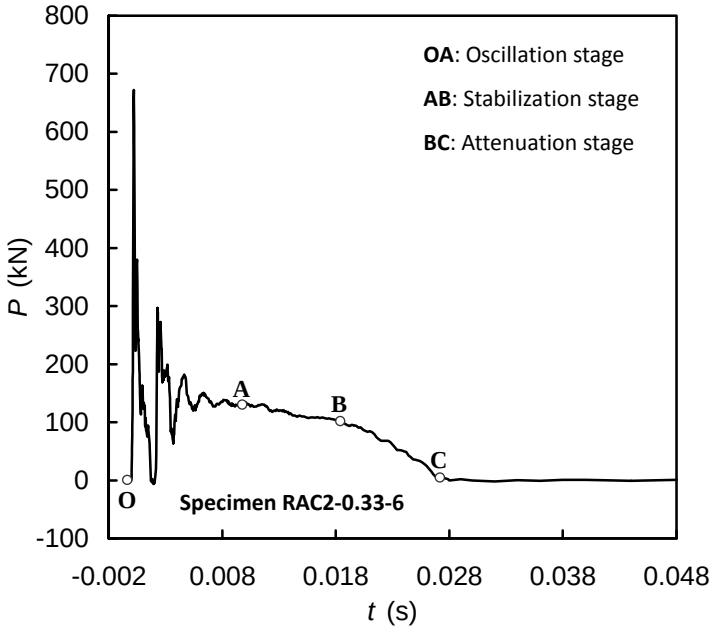

Fig. 8. Typical time history of impact loads.

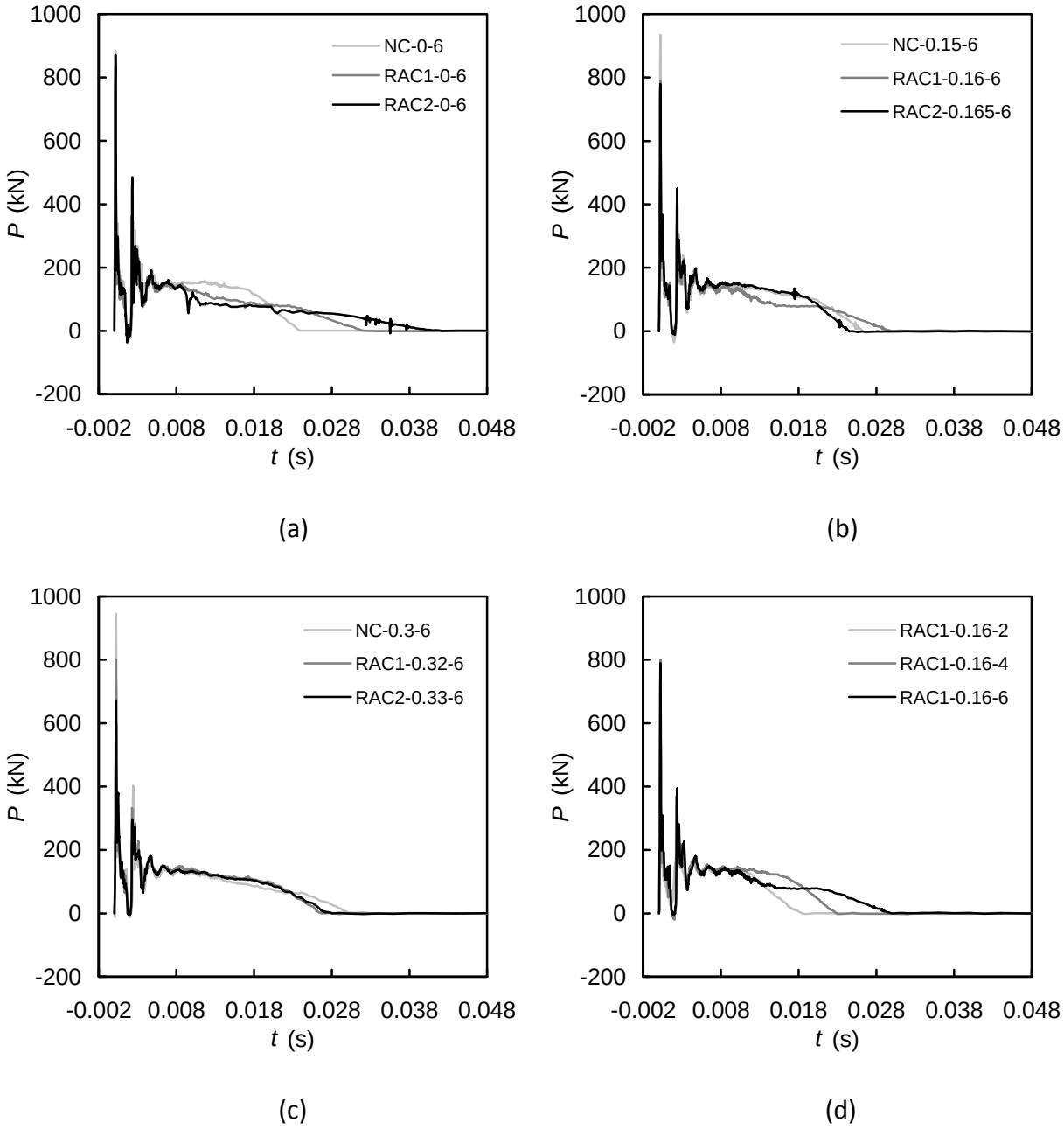

Fig. 9. Impact load-time history curve of the specimens.

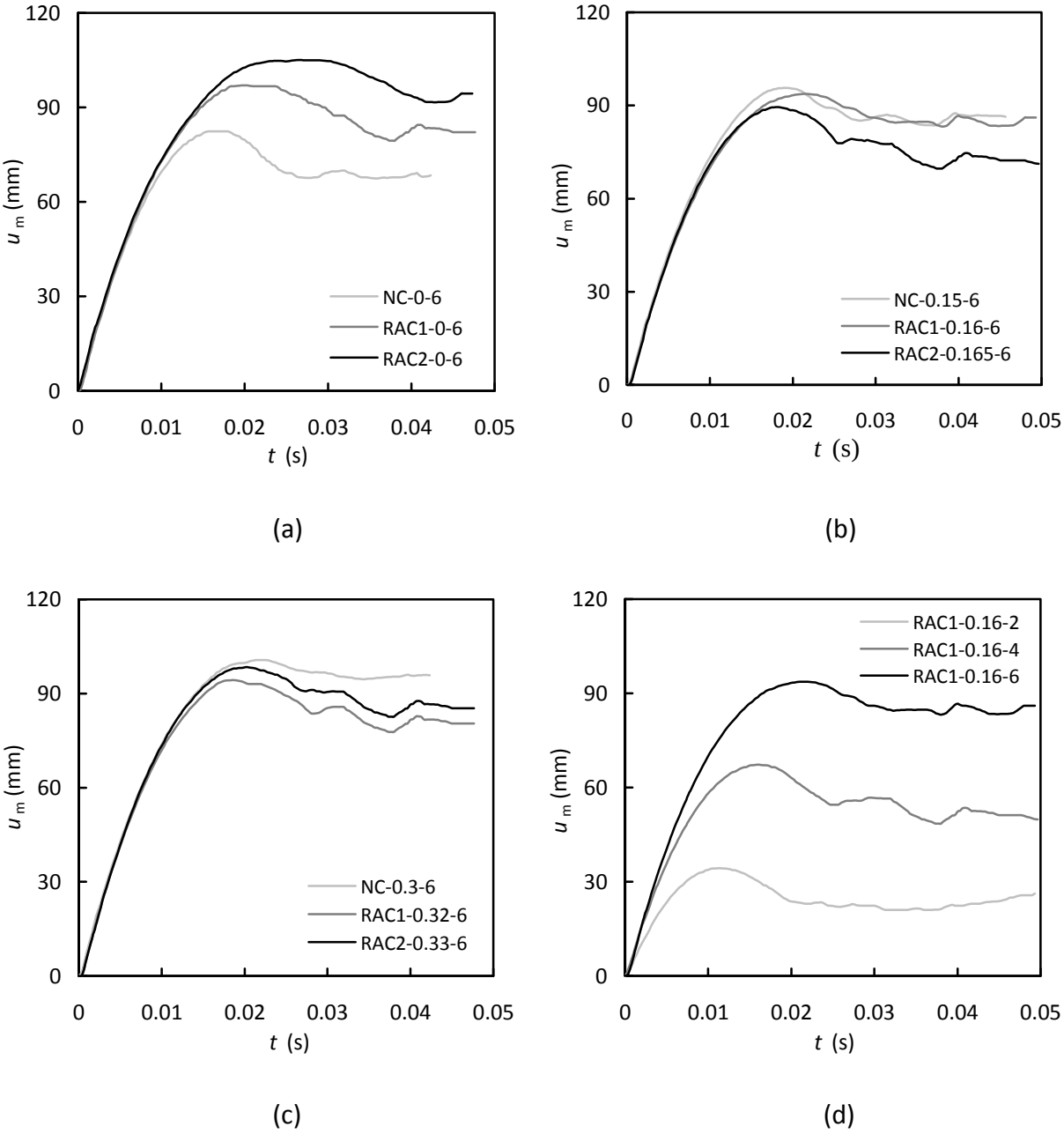

Fig. 10. Time histories of mid-span displacement.

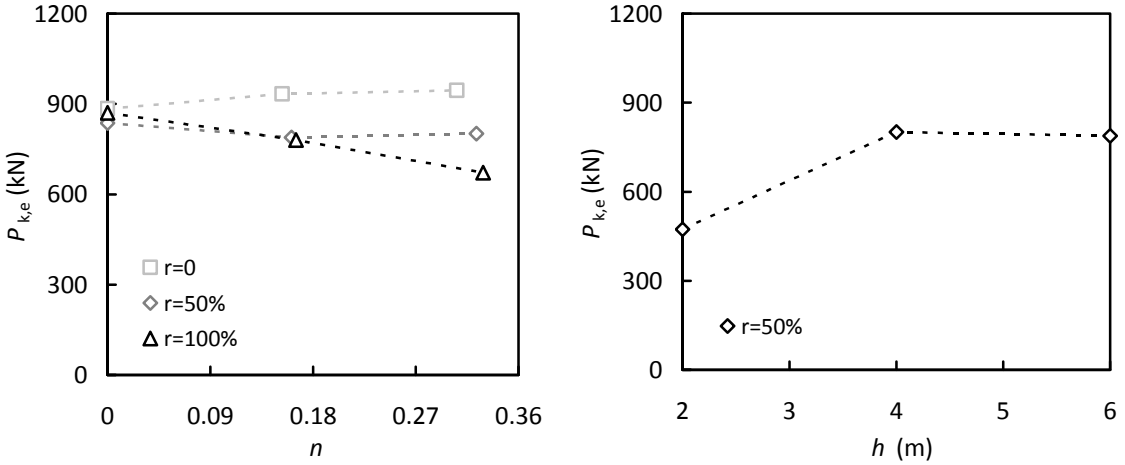

(a)

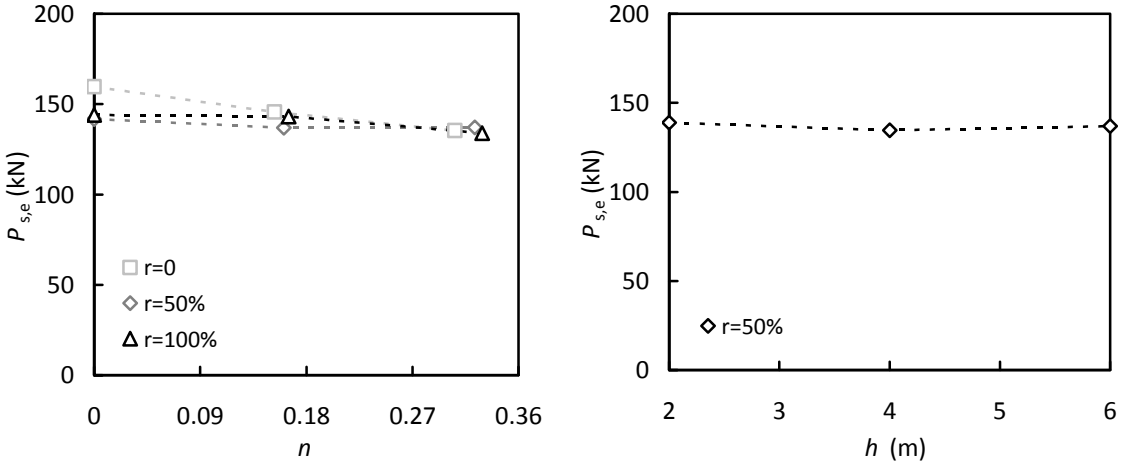

(b)

Fig. 11. Variation of $P_{k,e}$ and $P_{s,e}$.

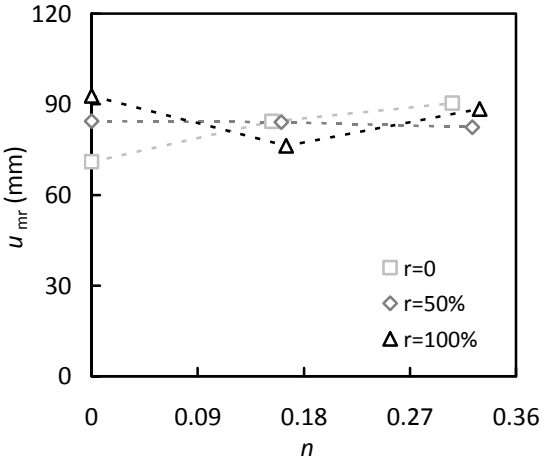

(a)

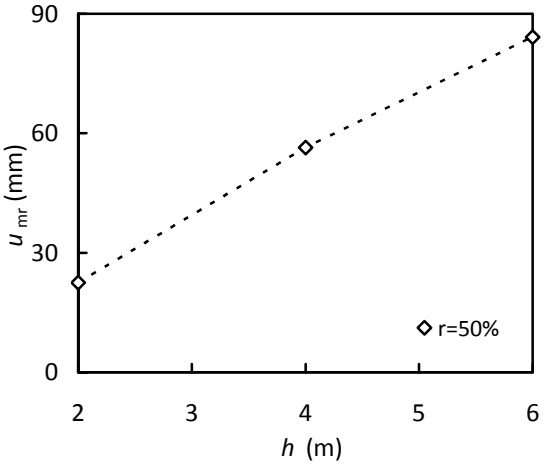

(b)

Fig. 12. Effect of typical parameters on u_{mr}.

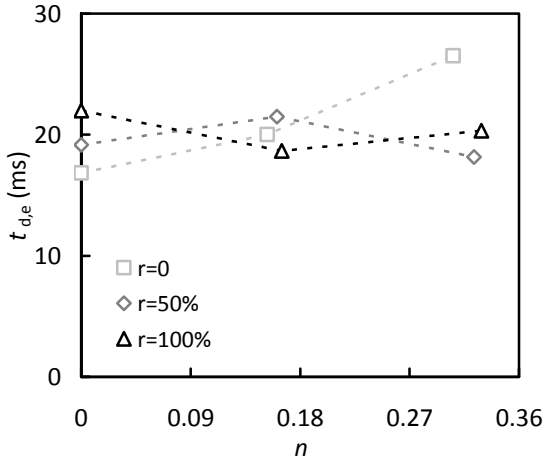

(a)

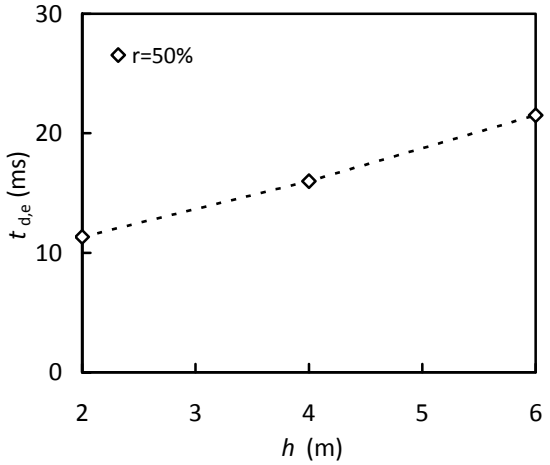

(b)

Fig. 13. Effect of typical parameters on $t_{d,e}$.

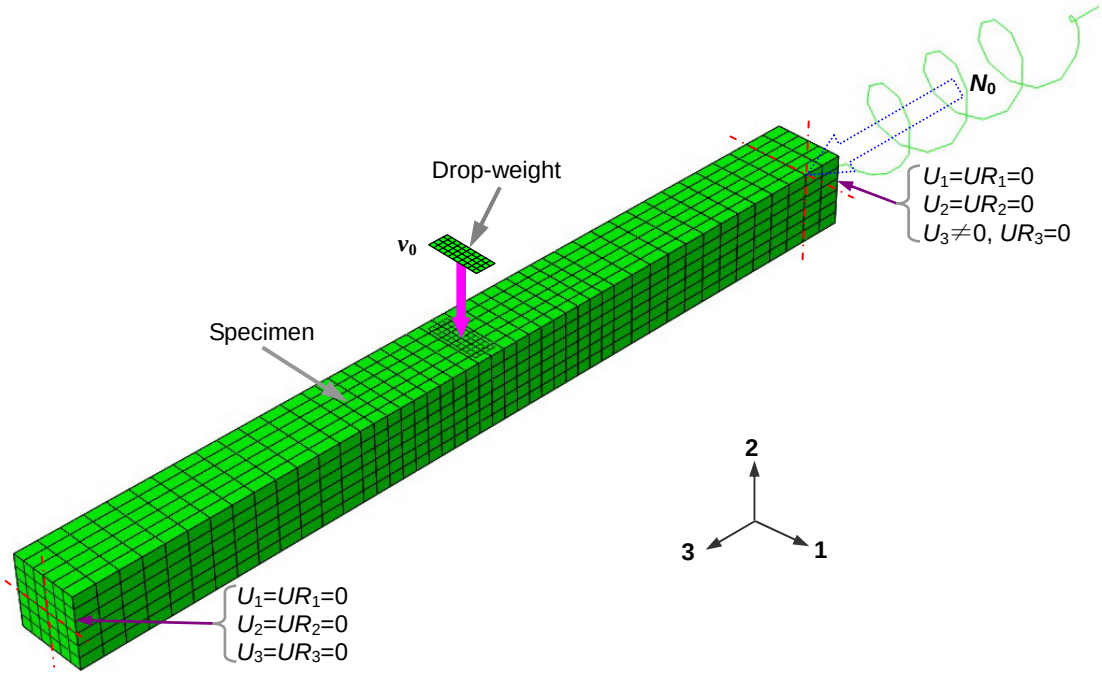

Fig. 14. Meshing and boundary conditions.

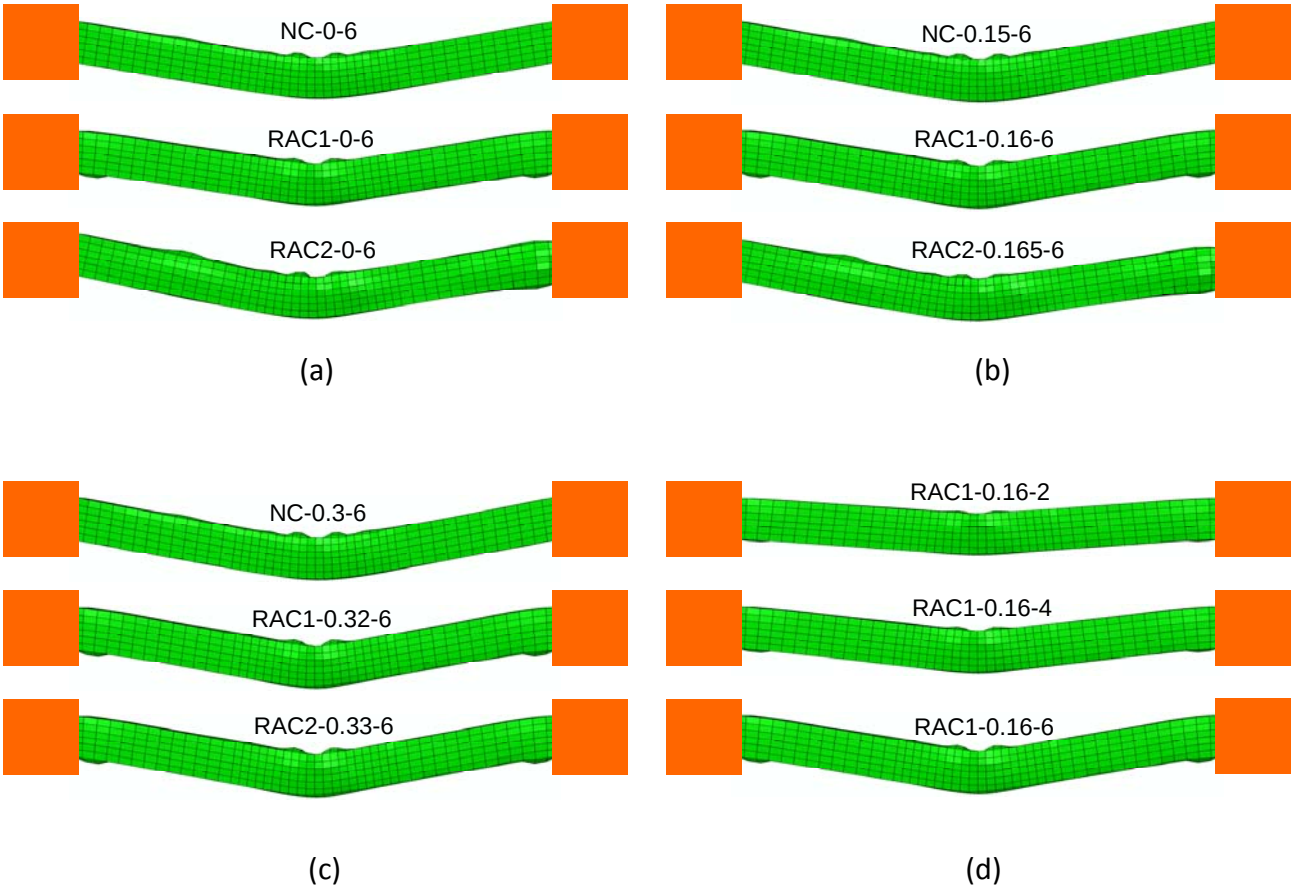

Fig. 15. Predicted failure patterns.

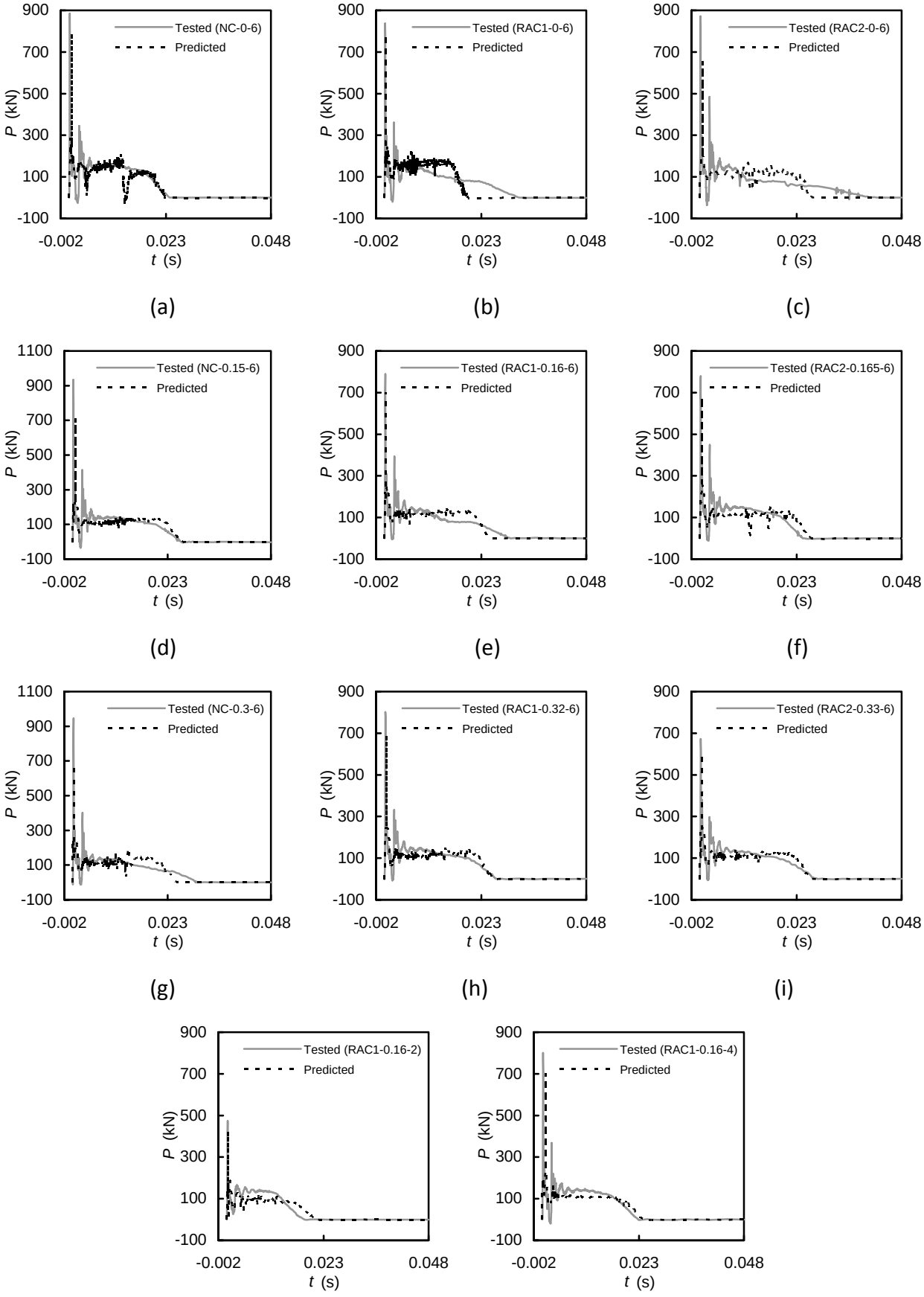

Fig. 16. Comparison between the predicted and tested $P-t$ history curves.

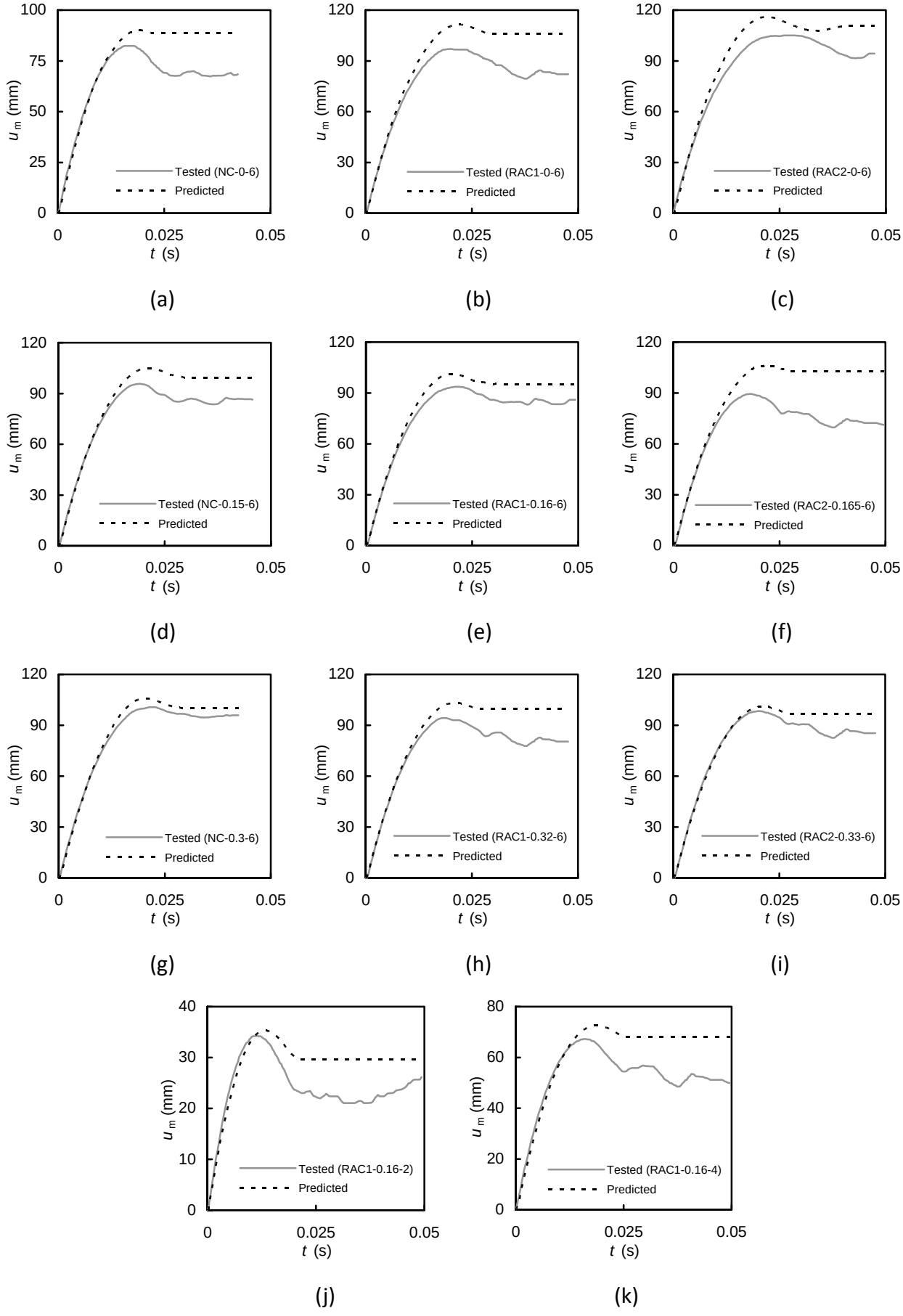

Fig. 17. Comparison between the predicted and tested $u_m - t$ curves.

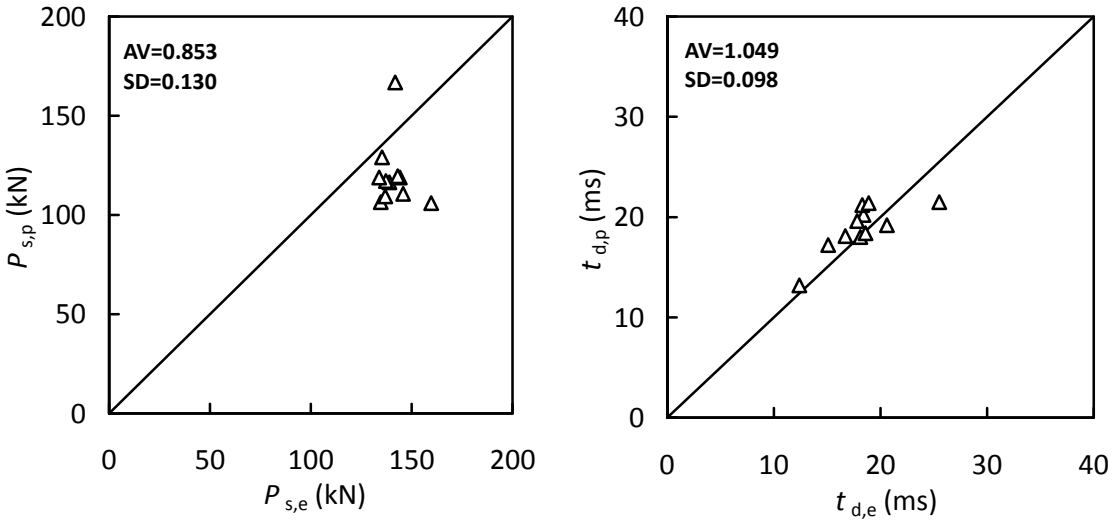

(a)

(b)

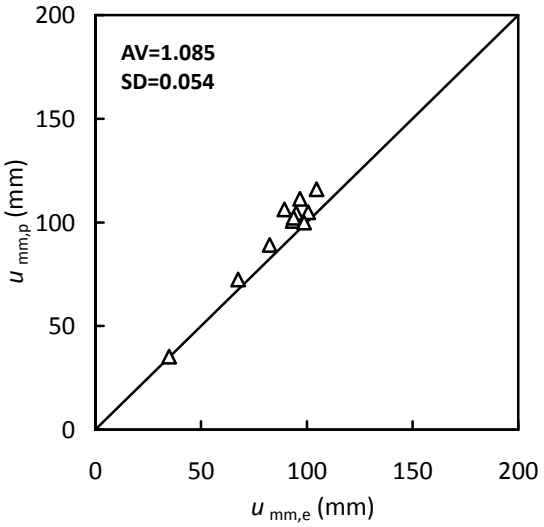

(c)

Fig. 18. Comparisons of P_s, t_d and u_{mm} between the predicted and experimental results.

Tables:

Table 1. Mix design and properties of fresh concrete.

Type	Cement (kg/m^3)	Sand (kg/m^3)	Coarse aggregate (kg/m^3)		Water (kg/m^3)	r (%)	Slump (mm)	$f_{cu,28}$ (MPa)	$f_{cu,test}$ (MPa)	E_c (N/mm^2)
			Nature	Recycled						
NC	473	636	1072	0	236.5	0	35	40.2	53.9	3.29×10^4
RAC	473	636	537	537	236.5	50	35	35.9	48.1	2.92×10^4
	473	636	0	1072	236.5	100	85	33.7	45.7	2.64×10^4

Table 2. Information of the specimens.

No.	Specimen label	$B\times t_s\times L$ (mm)	L_0 (mm)	r (%)	h (m)	N_0 (kN)	n	W (J)	$t_{d,e}$ (ms)	$P_{k,e}$ (kN)	$P_{s,e}$ (kN)	$u_{mm,e}$ (mm)	u_{mr} (mm)	Failure mode*
1	NC-0-6	100×2.45×1800	1200	0	6	0	0	14018.1	16.85	884.6	159.6	82.4	71.0	A+B
2	RAC1-0-6	100×2.45×1800	1200	50	6	0	0	14018.1	20.00	836.5	141.8	97.0	84.4	A+B+C
3	RAC2-0-6	100×2.45×1800	1200	100	6	0	0	14018.1	26.50	871.0	144.1	105.0	92.8	A+B+C
4	NC-0.15-6	100×2.45×1800	1200	0	6	100	0.15	14018.1	19.16	933.3	145.7	95.7	84.3	A+B
5	RAC1-0.16-6	100×2.45×1800	1200	50	6	100	0.16	14018.1	21.50	788.6	136.9	93.7	84.1	A+B
6	RAC2-0.165-6	100×2.45×1800	1200	100	6	100	0.165	14018.1	18.16	780.3	143.1	89.4	76.3	A+B
7	NC-0.3-6	100×2.45×1800	1200	0	6	200	0.3	14018.1	22.00	945.0	135.3	100.7	90.3	A+B
8	RAC1-0.32-6	100×2.45×1800	1200	50	6	200	0.32	14018.1	18.67	801.6	137.2	94.3	82.4	A+B
9	RAC2-0.33-6	100×2.45×1800	1200	100	6	200	0.33	14018.1	20.33	672.2	133.9	98.4	88.4	A+B
10	RAC1-0.16-2	100×2.45×1800	1200	50	2	100	0.16	4672.7	11.33	473.1	138.9	34.3	22.5	A
11	RAC1-0.16-4	100×2.45×1800	1200	50	4	100	0.16	9345.4	16.00	800.6	134.6	67.2	56.4	A+B

*A: buckling of steel tube at the compression side of the section near the mid-span; B: buckling of steel tube at the compression side of the section near the supports; and C: tensile facture of steel tube at the tension side of the mid-span section.